Solid State Electronics 146 (2018) 1–8

Contents lists available at ScienceDirect

Solid State Electronics

journal homepage: www.elsevier.com/locate/sse

A novel empirical *I-V* model for GaN HEMTs

Jie Yang[1,*], Yeting Jia[1], Ning Ye, Shuo Gao

ARTICLE INFO

The review of this paper was arranged by Prof. S. Cristoloveanu

Keywords:
GaN HEMT
Empirical *I-V* model
Self-heating effect
Trapping effects

ABSTRACT

In this paper, a novel eight-parameter empirical nonlinear current-voltage (*I-V*) model for gallium nitride (GaN) high electron mobility transistors (HEMTs) is presented. A hyperbolic sine function is introduced in this model to describe the transfer characteristics between drain-source current, I_{ds}, and gate-source voltage, V_{gs}. The self-heating and trapping effects have been considered and incorporated into the proposed model through expansion parameters. The proposed model has been verified on four different types of GaN HEMTs with good agreements between the simulated curves and the measured data. Comparison between the proposed model and other traditional non-square-law models indicates a significant accuracy improvement especially in linear region by the proposed model. This simple but accurate empirical *I-V* model can be easily implemented for computer aided circuit design and simulation with GaN HEMTs.

1. Introduction

In recent years, gallium nitride (GaN) high electron mobility transistors (HEMTs) become increasingly available and prove themselves as promising candidates for high power, high frequency and high temperature applications, due to their excellent physical properties of wide band gap, high critical breakdown field, high electron mobility and so forth [1]. To make full use of these superior properties of GaN HEMT devices, accuracy device models of GaN HEMTs are expected to facilitate the computer aided circuit design and simulation. Detailed, physics based three-dimensional (3-D) or two-dimensional (2-D) analytical models with numerous parameters are generally too complex to be used as circuit analysis tools, while simple, compact, and robust empirical *I-V* models with minimal parameters are more suitable for such kind of tasks.

Given the physics similarities of GaN and GaAs materials, it is interesting to survey some classic models originally developed for GaAs MESFETs and HEMTs. Extensive research efforts have been made to model GaAs devices, including the Curtice model, the Statz model, the Kacprzak-Materka model, the Rodriguez model, the Ahmed model, the Angelov model, the Curtice cubic model, and more [2–19]. The Curtice model [2], based on the Shichmann-Hodges JFET model [3], introduces the hyperbolic tangent function to integrate drain-source current, I_{ds}, in both linear region and saturation region into a uniform current equation. However, the accuracy of the Curtice model decreases in the low current region especially when the device is scaled down. The Rodriguez model [4], as an improved form of the Curtice model, can model the characteristics of devices in the low current region better by introducing the drain-source bias dependent pinch-off potential. The Materka model [5], proposed for large-signal depletion devices at moderate frequencies, can simulate the behavior of the short channel devices in saturation region [6,7]. Rodriguez et al. [8] compared the accuracy of the classical models and found out that the Materka model appeared to be more accurate than other models mentioned before in both linear region and saturation region, but its accuracy degraded severely for the submicron range MESFETs [9]. Ahmed et al. [10] modified the Materka model and predicted the behavior of the submicron GaAs MESFETs by introducing the concept of threshold voltage displacement due to the drain-source voltage (V_{ds}). In the Statz model [11], non-square relationship between I_{ds} and the gate-source voltage (V_{gs}) is described by adding a dopant tailing parameter into the model. But it fails to predict characteristics of devices at low current region where V_{gs} is near cutoff. The Islam-Zaman model [12], based on the Ahmed model, introduces an additional parameter to describe the effect of V_{gs} on the output conductance in saturation region, which shows better accuracy with excellent scalability for various device sizes. In the Curtice cubic model [13], a cubic polynomial equation is adopted to describe the relationship between I_{ds} and V_{gs} with a set of expansion parameters, but the physical explanation of these additional parameters remain uncertain. Dobes and Pospisil [14] used a variable at the exponential term of polynomial function instead of a square to provide flexibility of curve fitting among various devices [15]. The TriQuint model [16], modified from the Statz model, provides an improved fit by introducing the parameter Q to model the non-square-law dependency of I_{ds} without increasing complexity. The Angelov model [17], in principle, can model high-order derivatives of the current-voltage

* Corresponding author.
E-mail address: yangjie@ise.neu.edu.cn (J. Yang).
[1] These authors contributed equally to this work and should be considered co-first authors.

https://doi.org/10.1016/j.sse.2018.04.004
Received 7 October 2017; Received in revised form 12 April 2018; Accepted 15 April 2018
Available online 25 April 2018

Table 1
List of frequently used *I-V* models.

No.	Model Name	Model Description
1	The Curtice model	$I_{ds} = \beta(V_{gs}-V_T)^2 \times \tanh(\alpha V_{ds})(1+\lambda V_{ds})$
2	The Statz model	$I_{ds} = \begin{cases} \frac{\beta(V_{gs}-V_T)^2}{1+b(V_{gs}-V_T)} \times \left[1-(1-\frac{\alpha V_{ds}}{3})^3\right](1+\lambda V_{ds}) 0 < V_{ds} < \frac{3}{\alpha} \\ \frac{\beta(V_{gs}-V_T)^2}{1+b(V_{gs}-V_T)}(1+\lambda V_{ds}) V_{ds} \geqslant \frac{3}{\alpha} \end{cases}$
3	The Materka model	$I_{ds} = I_{dss}\left(1-\frac{V_{gs}}{V_T+\gamma V_{ds}}\right)^2 \times \tanh\left(\frac{\alpha V_{ds}}{V_{gs}-V_T-\gamma V_{ds}}\right)$
4	The Ahmed model	$I_{ds} = I_{dss}\left(1-\frac{V_{gs}}{V_T+\Delta T+\gamma V_{ds}}\right)^2 \times \tanh(\alpha V_{ds})(1+\lambda V_{ds})$
5	The Islam-Zaman model	$I_{ds} = I_{dss}\left(1-\frac{V_{gs}}{V_T+\Delta T+\gamma V_{ds}}\right)^2 \times \tanh(\alpha V_{ds})(1+\lambda V_{ds}+\mu V_{gs})$
6	The Angelov model	$I_{ds} = I_{pk}(1+\tanh(\varphi))\tanh(\alpha V_{ds})(1+\lambda V_{ds})$ $where\ \varphi = P_1(V_{gs}-V_{pk}) + P_2(V_{gs}-V_{pk})^2 + \cdots$
7	The Rodriguez model	$I_{ds} = \beta(V_{gs}-V_T-\gamma V_{ds})^2 \times \tanh(\alpha V_{ds})(1+\lambda V_{ds})$
8	The Curtice cubic model	$I_{ds} = (A_0 + A_1 V_1 + A_2 V_1^2 + A_3 V_1^3) \times \tanh(\alpha V_{ds}(t))$ $where\ V_1 = V_{gs}(t-\tau)[1+\beta(V_{ds}^o - V_{ds}(t))]$
9	The TriQuint model	$I_{ds} = \frac{I_{ds0}}{1+\delta I_{ds0}}$ $where\ I_{ds0} = \begin{cases} \beta(V_{gs}-V_T-\gamma V_{ds})^Q \times \left[1-\left(1-\frac{\alpha V_{ds}}{3}\right)^3\right] & 0 < V_{ds} < \frac{3}{\alpha} \\ \beta(V_{gs}-V_T-\gamma V_{ds})^Q & V_{ds} \geqslant \frac{3}{\alpha} \end{cases}$
10	The Dobes-Pospisil model	$I_{ds} = \beta(V_{gs}-V_T-\gamma V_{ds})^n \times \tanh(\alpha V_{ds})(1+\lambda V_{ds})$
11	The Proposed model	$I_{ds} = \sinh(\gamma(V_{gs}-V_{T0}-\delta V_{ds})^n) \times \tanh((\alpha_0+\alpha_1 V_{gs}+\alpha_2 V_{ds})V_{ds})(1+\lambda V_{ds}+\mu V_{gs})$

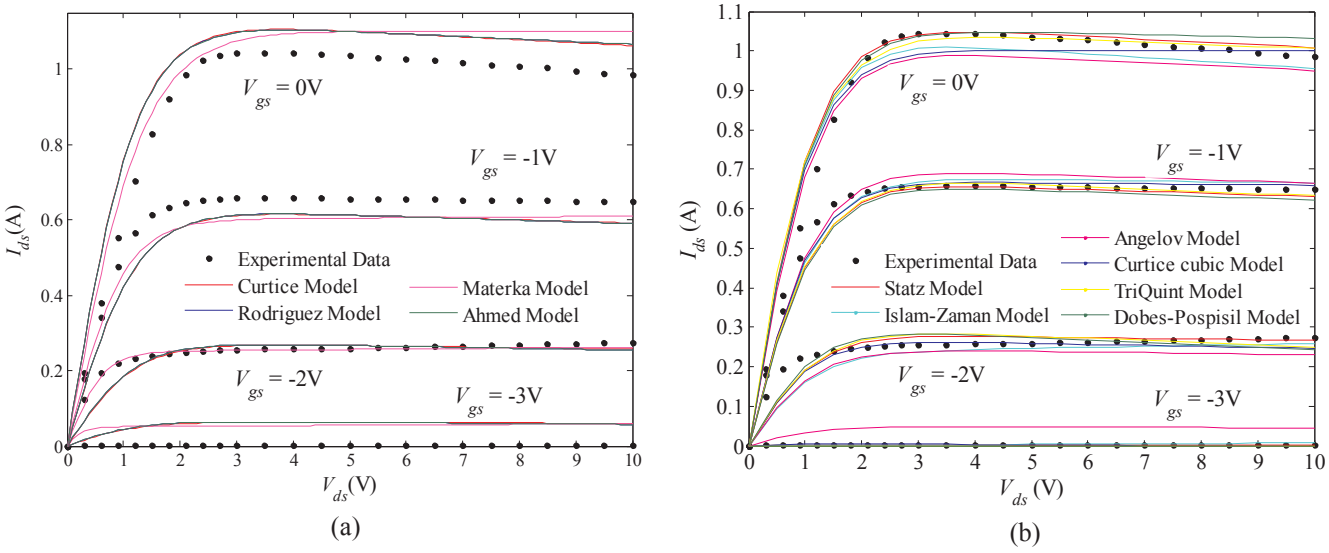

Fig. 1. The measured data and the simulated output characteristics of CGH60008D bare die from square-law and non-square-law models, (a) square-law models; (b) non-square-law models.

characteristic by introducing the hyperbolic tangent function to model the dependency of I_{ds} on V_{gs}, which is widely used by virtue of its good convergence and simple parameter extraction [18]. However, the parameter extraction is sensitive to the initial values and may trapped into local optima. Besides, good accuracy of the model can be achieved only when the drain-source bias voltage is fixed [19].

Unlike MESFETs, two types of materials with different band gaps form a heterojunction. Two dimensional electron gas (2DEG), i.e., the channel, is created near the interface of the two materials when a large number of electrons are transferred from the highly doped material with higher band gap to the material with lower band gap [20]. It has been previously shown that effects induced by spontaneous and piezoelectric polarization can have a substantial influence on the concentration, distribution and recombination of free carriers in strained group III nitride heterostructures [21,22]. Therefore, the traditional empirical *I-V* models, mainly developed for GaAs MESFETs and HEMTs, are not adequate to model the characteristics of emerging GaN HEMTs.

The aim of this paper is to present an accurate and simple empirical model for GaN HEMTs. A novel hyperbolic sine relationship was introduced to describe the actual transfer behavior of the devices in our model. In addition, the mechanisms of self-heating and trapping effects were analyzed and numerically defined in the proposed model by additional expansion parameters instead of using complex electro-thermal sub-circuit. Comparisons were made between the proposed model and traditional empirical *I-V* models to verify the applicability and accuracy of the proposed model.

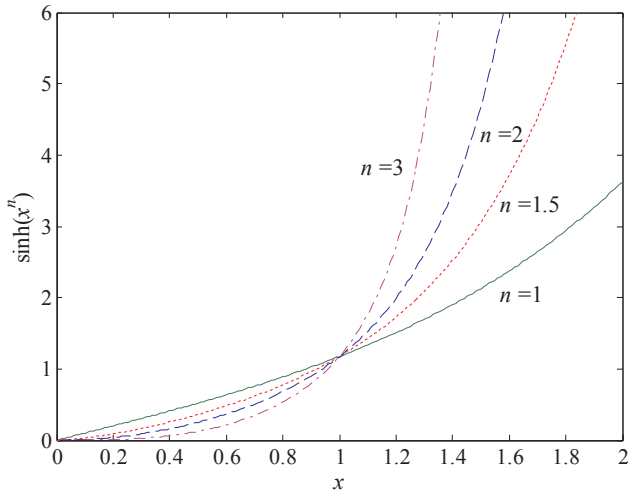

Fig. 2. The shapes of hyperbolic sine function $\sinh(x^n)$ with different exponent parameter n.

2. Device measurement

Four different off-the-shelf GaN HEMT devices from three manufacturers are adopted in this study: CGH60008D bare die from Cree, Inc., CGH40010F in ceramic/metal flange package from Cree, Inc., QPD1010 in 3 × 3 mm surface mount QFN package from Qorvo, Inc., and NPTB00004A with standard SOIC plastic package from MACOM, Inc. These devices have different dimensions which would significantly affect their characteristics. The proposed model, however, should predict device characteristics regardless of size, or for a given device size the model should predict the characteristics for all the variables, which can be changed during fabrication. For a rigorous device model, the parameter values will change corresponding to the devices types, but the model itself should remain valid. Therefore, the purpose of selecting these devices is to verify the applicability of the proposed model for various types of GaN HEMTs.

The *I-V* characteristics of the four GaN HEMTs were measured using STI 5300C semiconductor curve tracer from Scientific Test, Inc., connected with SemiShare SE probe station from Semishare Electronic Co., Ltd. Two sets of curves were captured for each device, namely output characteristics and transfer characteristics. For output characteristic curves, V_{ds} swept from 0 V to 10 V while V_{gs} varied from −3 V to 0 V in step of 1 V (V_{gs} varied from −1.5 V to 0 V in step of 0.5 V for NPTB00004A). For transfer curves, V_{gs} swept from −3.5 V to 0 V (from −2.5 V to 0 V for NPTB00004A) while V_{ds} was set to 1 V and 5 V. *I-V* curves of the devices were measured in static mode and the dwell time of each sample was 50 ms. The effect of self-heating on transistor characteristics can be apparent with significant values of thermal resistance. The static current sags greatly at large values of power dissipation. The output conductance G_{ds} and the transconductance G_m were also calculated by taking the numerical differentiation of I_{ds} with respect to V_{ds} and V_{gs}, respectively. In addition, the threshold voltages were obtained from terminal measurements of the devices according to manufacturer's test condition specifications.

3. Comparison of traditional *I-V* models

The mathematical expressions of ten frequently used *I-V* models mentioned in the previous section are summarized in Table 1. These models were applied to CGH60008D GaN HEMT bare die (for which the influences of packaging to the *I-V* characteristics of the device is minimized) to test their performances. The identical curve-fitting procedure based on the least-square (LS) approach was applied on all models to extract the optimal parameter values. Depending on the current-voltage relationship in saturation region, these models can be generally classified into two categories: square-law models and non-square-law models. The simulated output characteristics of the former group of models, including the Curtice model, the Rodriguez model, the Materka model, the Ahmed model, are depicted in Fig. 1(a); while the simulated output characteristics of the latter group of models are depicted in Fig. 1(b), including the Statz model, the Islam-Zaman model, the Angelov model, the Curtice cubic model, the TriQuint model and the Dobes-Pospisil model.

Fig. 1 clearly indicates that the square-law models are not suitable for GaN HEMT devices, while the non-square-law models have significant advantages over the square-law models in general, which may be attribute to the higher order terms from the Taylor series expansion of non-square-law models. All non-square-law models can simulate the behavior of the device in saturation region reasonably well, especially the Statz model and its derivative, the TriQuint model. The self-heating effect cannot be characterized in some non-square-law models that lack the terms to describe the negative correlation between I_{ds} and V_{ds} in saturation region when V_{gs} is high. However, a common issue of these non-square-law models is that the noticeable deviation between the predicted values and measured data can be observed in linear region, which could be associated with the poor control in modulating I_{ds} for small V_{ds}. Although the GaN HEMT devices normally operate in saturation region in practical applications, it is still always desirable to establish an accurate *I-V* model with superior performance in linear region as well for some particular applications, such as voltage controlled amplifiers.

4. Derivation of the proposed model

To simplify the problem, the drain current I_{ds}, which is a function of both V_{ds} and V_{gs}, is assumed to be a product of two functions in the beginning as follows:

$$I_{ds}(V_{gs},V_{ds}) = f(V_{gs})g(V_{ds}) \tag{1}$$

where $f(V_{gs})$ and $g(V_{ds})$ are the current components depending on only V_{gs} and V_{ds}, respectively. $f(V_{gs})$ is obtained from the transfer characteristic of the GaN HEMTs. By examining the shapes of transfer characteristic curves carefully with numerous mathematic functions, we discovered that the hyperbolic sine function might be a better match to describe the relationship between I_{ds} and V_{gs}. For illustration, the function $y = \sinh(x^n)$ with different values of exponent parameter n are depicted in Fig. 2. By varying the value of n, the tilt of the curve can be adjusted to closely approximate the measured data. The proper value of n is normally from 1.5 to 2.5.

Thus, the drain current component $f(V_{gs})$ is defined as:

$$f(V_{gs}) = \sinh(\gamma(V_{gs}-V_T)^n) \tag{2}$$

Table 2
Parameters of the proposed model for different devices.

	V_{T0}	γ	δ	α_0	α_1	α_2	λ	μ	n	R^2
CGH60008D	−2.952	−0.1565	−0.008115	−0.5181	0.3909	−0.116	−0.01298	−0.3627	1.646	0.9996
CGH40010F	−2.849	−0.2275	−0.008447	−0.5061	0.3265	−0.03979	−0.01362	−0.7753	1.844	0.9995
QPD1010	−2.799	−0.18	−0.02453	−0.3781	0.2969	−0.04504	−0.0142	−0.3723	1.5	0.9991
NPTB00004A	−1.704	−0.2184	−0.01813	−0.615	0.8073	−0.1207	−0.02195	−0.6521	2.001	0.9992

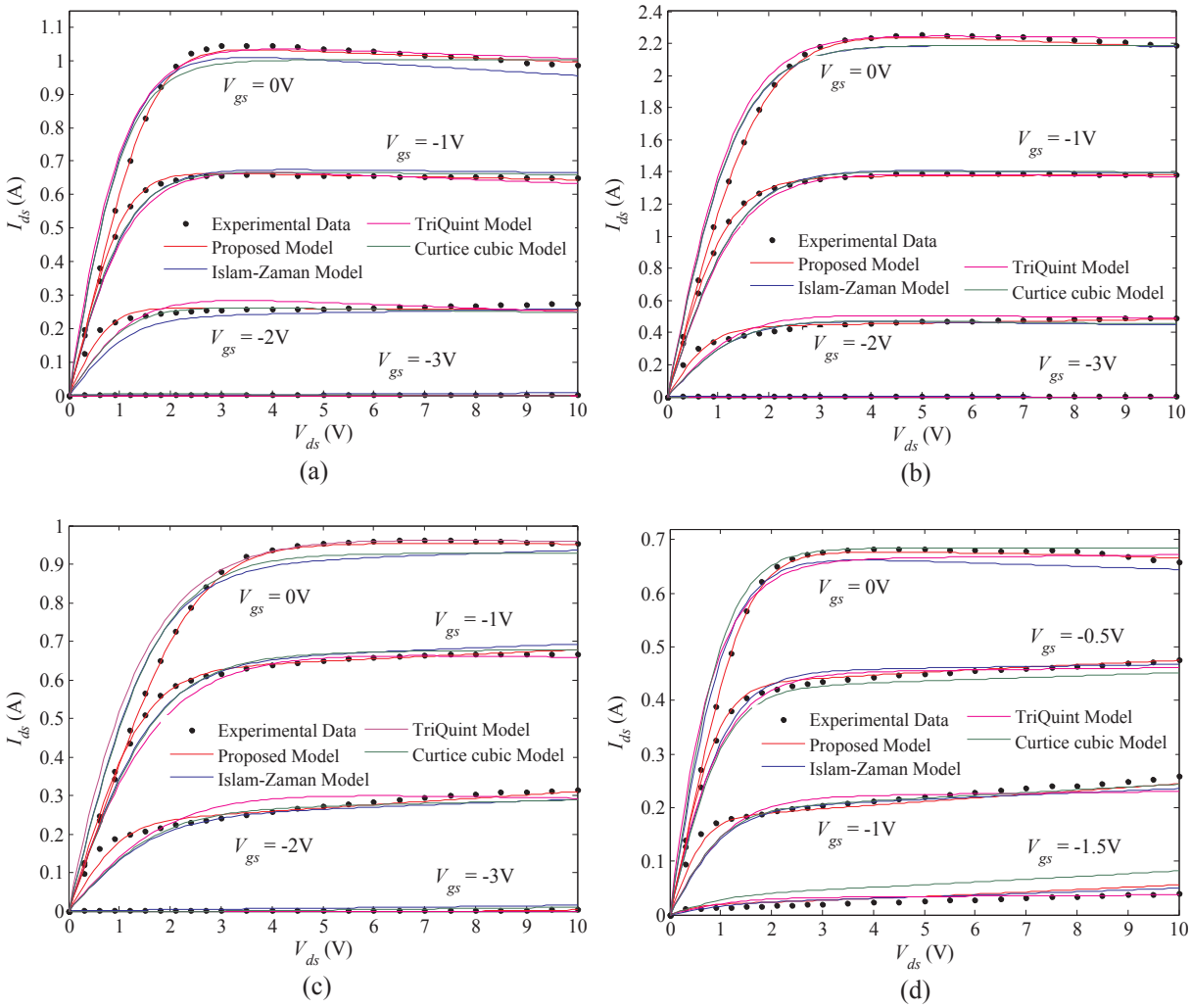

Fig. 3. Measured and simulated output characteristics for four GaN HEMTs, (a) CGH60008D; (b) CGH40010F; (c) QPD1010; (d) NPTB00004A.

Table 3
RMS errors of models.

	Islam-Zaman model	Curtice Cubic model	TriQuint model	Proposed model
CGH60008D	0.02133	0.02093	0.01951	0.007025
CGH40010F	0.04059	0.0401	0.04111	0.01662
QPD1010	0.0231	0.02239	0.02445	0.009381
NPTB00004A	0.01649	0.02539	0.01807	0.006788

where V_T is the threshold voltage, γ and n are the two empirical shaping parameters. As suggested in [6], a small threshold voltage displacement is experienced when a drain bias voltage V_{ds} is applied. To reach a better approximation, the threshold voltage displacement should also be incorporated into Eq. (2) as follows:

$$f'(V_{gs},V_{ds}) = \sinh(\gamma(V_{gs}-V_{T0}-\delta V_{ds})^n) \tag{3}$$

where δ is the threshold voltage displacement parameter.

To model the drain current dependency on V_{ds}, a uniform hyperbolic tangent function covering both linear and saturation regions is frequently used, which is given by:

$$g(V_{ds}) = \tanh(\alpha V_{ds})(1 + \lambda V_{ds}) \tag{4}$$

where parameter α determines the voltage at which I_{ds} saturates, and λ is the channel modulation parameter. However, Eq. (4) is not adequate to describe the self-heating and trapping effects which are particularly prominent for GaN HEMTs. GaN HEMTs generally operate at depletion mode. there are two primary types of trapping effects in GaN HEMTs: the surface trap and the substrate trap. The existence of the substrate trap would produce a drain-lag effect, i.e., a slow change in the drain-source current in response to the increase of the drain-source voltages [23]. Similarly, the surface trap can cause a gate-lag effect. This surface state will create a virtual gate toward the drain terminal [24]. The two trapping effects are the combined results from the increments of both V_{ds} and V_{gs} in the knee region. As such, the parameter α in Eq. (4) is replaced by $(\alpha_0 + \alpha_1 V_{gs} + \alpha_2 V_{ds})$ to incorporate these effects and obtains a better fit to the measured static characteristics.

With the higher gate-source voltage, the 2DEG density becomes higher. Electrons are more likely to be captured by the substrate trap when the device operates in saturation region, resulting in a drain-source current loss. In addition, when the device operated in the continuous mode, the channel temperature will increase due to heat generated in the device channel from power dissipation and thermal conductivity decrease. It will further decrease I_{ds}, which is so called the self-heating effect. The effect of self-heating is particularly important for devices capable of high power applications. An effective approach is to use pulsed *I-V* measurement to isolate the self-heating, then include a dedicated thermal sub-circuit in the equivalent circuit model of the device to model the current change due to self-heating effect [25–29]. However, the pulsed *I-V* testing setup may not be easily available, and the device model becomes more complex. It is observed that the self-heating phenomenon can be represented by a pronounced negative

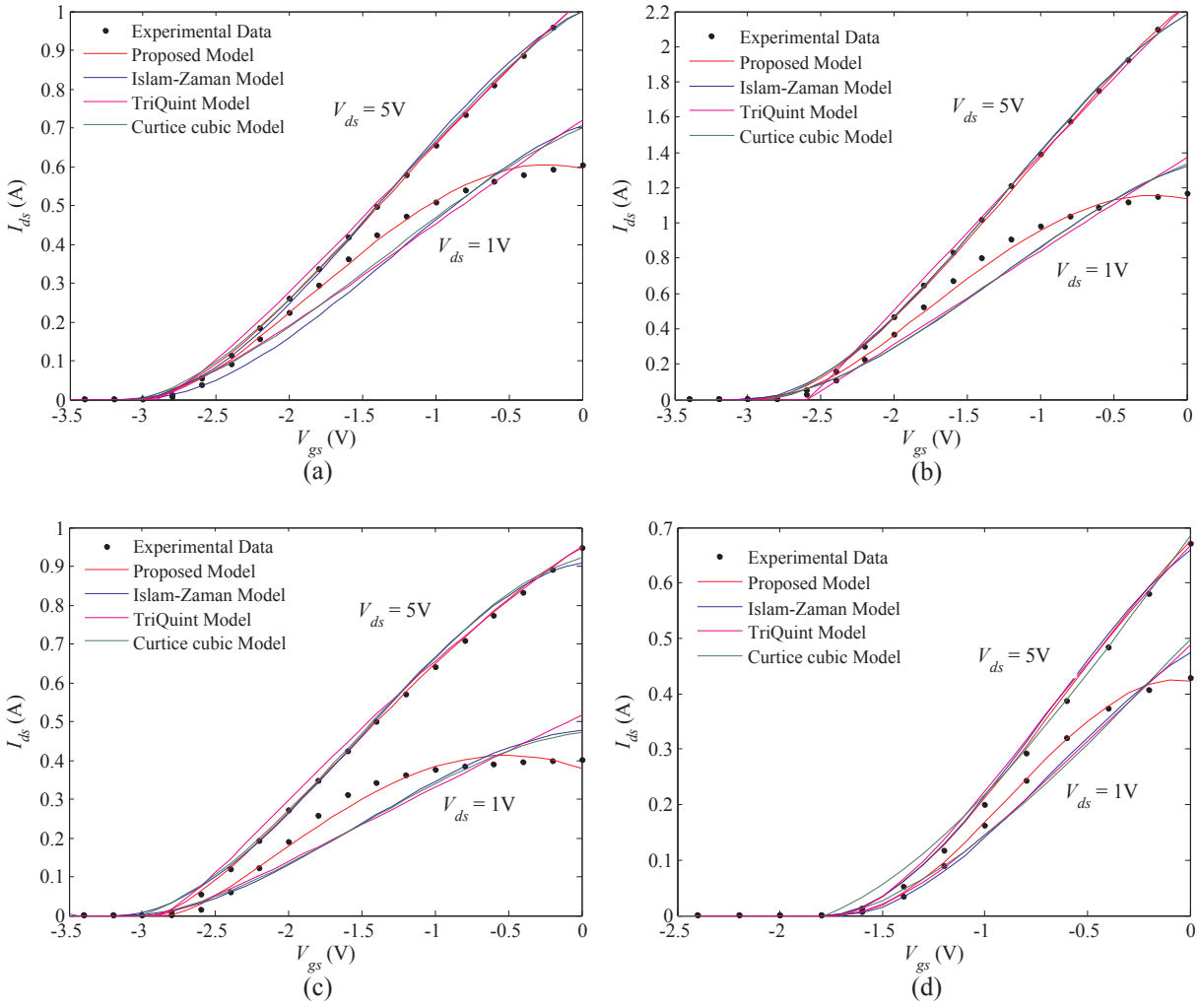

Fig. 4. Measured and simulated transfer *I-V* characteristics for four GaN HEMTs, (a) CGH60008D; (b) CGH40010F; (c) QPD1010; (d) NPTB00004A.

slope in saturation region of *I-V* characteristics as the drain voltage increases. By introducing a new fitting parameter, this negative slope can be captured so current change due to self-heating can be directly reflected in our empirical model. Therefore, the proposed model provides a simple yet accurate alternative of self-heating modeling without requiring pulsed *I-V* testing and additional thermal sub-circuit. Based on the above analysis, we can conclude that the output conductance G_{ds} in saturation region is sensitive not only to V_{ds} but also to V_{gs}. Thus, the term $(1 + \lambda V_{ds})$ in Eq. (4) is replaced by $(1 + \lambda V_{ds} + \mu V_{gs})$ to describe the modulation of I_{ds} by V_{gs} in saturation region.

Taking the above mentioned self-heating and trapping effects into account, the second current component is also a function of both V_{gs}, and V_{ds}. Thus Eq. (4) is revised as:

$$g'(V_{ds},V_{gs}) = \tanh((\alpha_0 + \alpha_1 V_{gs} + \alpha_2 V_{ds})V_{ds})(1 + \lambda V_{ds} + \mu V_{gs}) \tag{5}$$

Finally, by combining Eq. (3) and Eq. (5), a new *I-V* model for GaN HEMTs is proposed:

$$I_{ds} = f'(V_{gs},V_{ds})g'(V_{ds},V_{gs}) = \sinh(\gamma(V_{gs}-V_{T0}-\delta V_{ds})^n) \times \tanh((\alpha_0 + \alpha_1 V_{gs} + \alpha_2 V_{ds})V_{ds})(1 + \lambda V_{ds} + \mu V_{gs}) \tag{6}$$

The output conductance and the transconductance of the GaN HEMTs can be derived from Eq. (6) by taking the partial derivative of I_{ds} respect to V_{ds} and V_{gs}, respectively:

$$\begin{aligned} G_{ds} = {} & \lambda\sinh(\gamma(V_{gs}-V_{T0}-\delta V_{ds})^n)\tanh((\alpha_0 + \alpha_1 V_{gs} + \alpha_2 V_{ds})V_{ds}) \\ & + \sinh(\gamma(V_{gs}-V_{T0}-\delta V_{ds})^n)(1-\tanh^2((\alpha_0 + \alpha_1 V_{gs} + \alpha_2 V_{ds})V_{ds}))(\alpha_0 \\ & + \alpha_1 V_{gs} + 2\alpha_2 V_{ds})(1 + \lambda V_{ds} + \mu V_{gs}) - (1 + \lambda V_{ds} \\ & + \mu V_{gs})\cosh(\gamma(V_{gs}-V_{T0}-\delta V_{ds})^n)\tanh((\alpha_0 + \alpha_1 V_{gs} \\ & + \alpha_2 V_{ds})V_{ds})n\gamma\delta(V_{gs}-V_{T0}-\delta V_{ds})^{n-1} \end{aligned} \tag{7}$$

$$\begin{aligned} G_m = {} & \mu\sinh(\gamma(V_{gs}-V_{T0}-\delta V_{ds})^n) \times \tanh((\alpha_0 + \alpha_1 V_{gs} + \alpha_2 V_{ds})V_{ds}) \\ & + \gamma n\cosh(\gamma(V_{gs}-V_{T0}-\delta V_{ds})^n)(V_{gs}-V_{T0}-\delta V_{ds})^{n-1}\tanh((\alpha_0 + \alpha_1 V_{gs} \\ & + \alpha_2 V_{ds})V_{ds})(1 + \lambda V_{ds} + \mu V_{gs}) + (1 + \lambda V_{ds} \\ & + \mu V_{gs})\sinh(\gamma(V_{gs}-V_{T0}-\delta V_{ds})^n)(1-\tanh^2((\alpha_0 + \alpha_1 V_{gs} \\ & + \alpha_2 V_{ds})V_{ds}))\alpha_1 V_{ds} \end{aligned} \tag{8}$$

It is worth emphasizing that a complete large-signal model generally includes extrinsic and intrinsic elements. The description of nonlinear current sources I_{ds} (V_{gs}, V_{ds}) is the most complex and critical part and is commonly used in circuit design. The main goal of the paper is to present an empirical model of GaN HEMTs that can describe the *I-V* behavior of the device accurately. The dynamic characteristics of the devices, which requires the modeling of parasitic elements, is beyond the scope of this paper.

5. Parameter extraction and validation

Once the experimental data for the four GaN HEMTs are obtained,

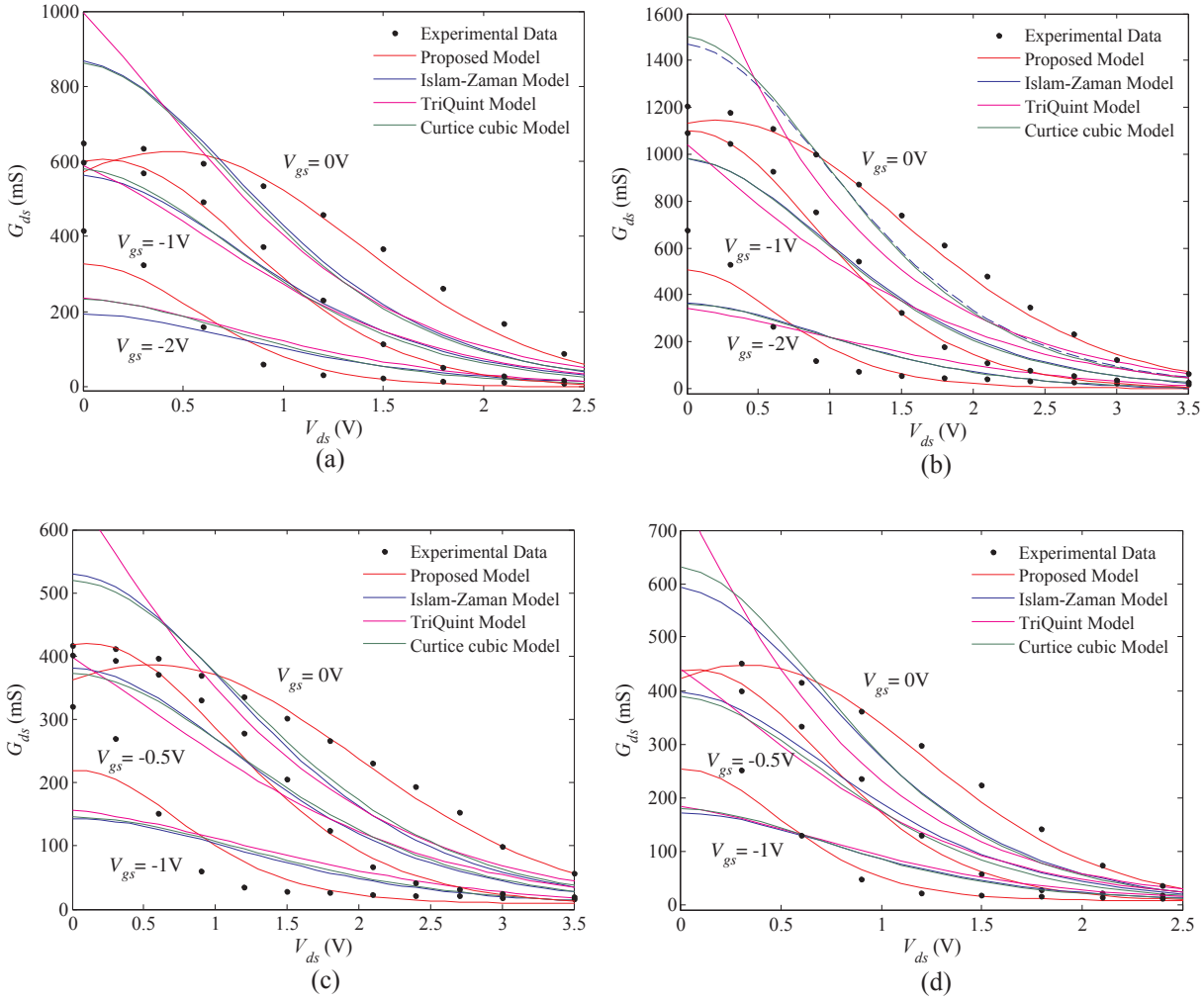

Fig. 5. Calculated and simulated output conductance G_{ds} for four GaN HEMTs, (a) CGH60008D; (b) CGH40010F; (c) QPD1010; (d) NPTB00004A.

the proposed model is applied to the experimental data to search for the best possible parameter values in the model. Since there are two independent control variables V_{gs} and V_{ds} and one response variable I_{ds}, surface fitting techniques would be required. To simplify the problem, we utilize the surface fitting toolbox provided by Matlab, based on LS approach, to optimize eight parameters (γ, δ, n, α_0, α_1, α_2, λ, μ) simultaneously. The parameters are optimized within the prescribed limits to ensure the extracted parameter values are reasonable and meaningful. The extracted parameter values of the proposed model for the four GaN HEMT devices and the $\mathbf{R}^2$ values, which are the statistical measures of goodness-of-fit of the proposed model corresponding to each device, are summarized in Table 2. The $\mathbf{R}^2$ is defined as:

$$\mathbf{R}^2 = 1 - \frac{\sum_{i=1}^{n} (y_i - \phi(x_i))^2}{\sum_{i=1}^{n} (y_i - \bar{y})^2} \tag{9}$$

where n is number of samples, y_i is the measured data for sample i, $\bar{y}$ is the mean value, and $\varphi(x_i)$ is the predicted value for the corresponding sample. For comparison, three relatively better non-square-law models inherited from different origins are selected from the model pool and applied to the same experimental data sets for parameter extraction. Fig. 3 shows the measured and simulated output characteristics from the proposed model, the TriQuint model, the Curtice cubic model and the Islam-Zaman model. The proposed model and the TriQuint model have close trajectories in saturation region for all of the four devices being tested, and their predictions are marginally better than that of the Curtice cubic model and the Islam-Zaman model. In linear region, however, the proposed model displays significant improvement over any other models in comparison and coincides with the measured characteristics perfectly. The $\mathbf{R}^2$ value of the proposed model ranges between 0.9991 and 0.9996 for these GaN HEMTs, which strongly confirms that our proposed model can predict the behaviors of these GaN HEMTs with extremely high degree of accuracy. The advantage of the proposed model over other models is also confirmed by the root-mean-square (RMS) errors calculated and summarized in Table 3. The RMS errors of the TriQuint model, the Curtice cubic model and the Islam-Zaman model are all comparable for the four GaN devices, while the RMS error of the proposed model is 64% lower than that of the second best TriQuint model for CGH60008D, 58.6% and 58.1% lower than that of the second best Curtice Cubic model for CGH40010F and QPD1010, and 58.8% lower than the second best Islam-Zaman model for NPTB00004A.

Fig. 4 shows the measured and simulated transfer *I-V* characteristics from the four models in comparison when V_{ds} is set to 1 V and 5 V. It can be observed that, as the devices operate in linear region, the drain-source current starts to saturate when V_{gs} is above a certain value. Only the proposed model can correctly interpret this phenomenon while other models still follow the same linearly increasing trend as in saturation region.

The advantage of the proposed model over the other three traditional models in linear region is more evident by examining the output conductance G_{ds} of the four GaN HEMTs, as illustrated in Fig. 5. For all four devices, the simulated output conductance curves are flatter and deviated from the experimental data when V_{gs} is either high or low. The

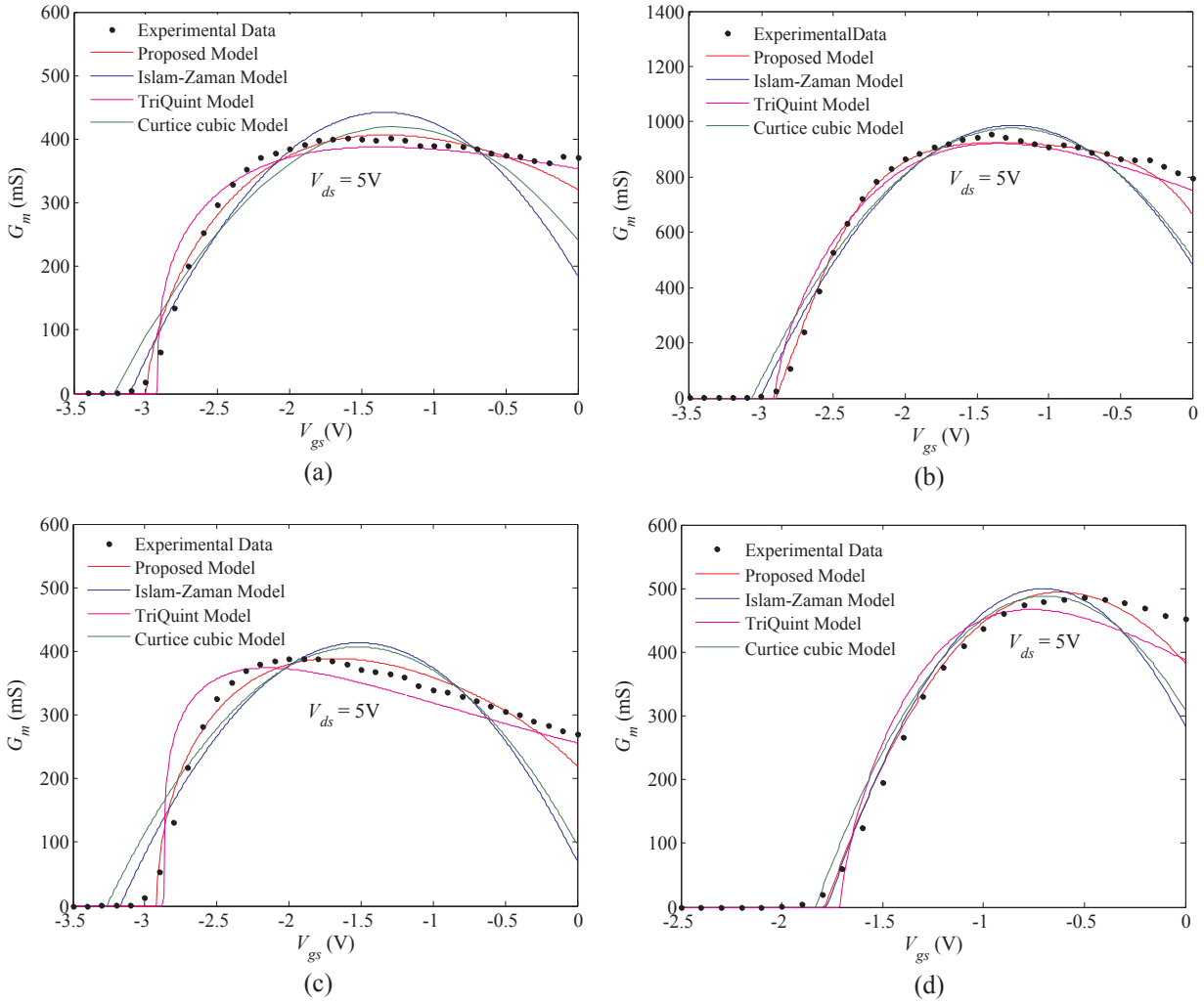

Fig. 6. Calculated and simulated G_m by different models for four GaN HEMTs, (a) CGH60008D; (b) CGH40010F; (c) QPD1010; (d) NPTB00004A.

proposed model, however, can resemble the detailed curvature structures of the experimental data with minimum deviation.

Finally, the calculated and simulated transconductance G_m of the GaN HEMTs in saturation region (V_{ds} = 5 V) from the four models are depicted in Fig. 6. The simulated transconductance curves of the Curtice cubic model and the Islam-Zaman model have classic "bell" shapes which is normally possessed by GaAs FETs [17]. Although the TriQuint model and the proposed model can successfully mimic the irregular step shapes of transconductance curves presented by GaN HEMTs, the proposed model outperforms the TriQuint model under majority of gate conditions except when V_{gs} is close to 0 V.

6. Conclusion

A practical, simple, yet accurate empirical *I-V* model for GaN HEMT devices is presented in the paper. A novel hyperbolic sine function is introduced in the model to describe the transfer *I-V* relationship of the GaN HEMT devices. In addition, self-heating and trapping effects are also analyzed and integrated into the proposed model through a set of expansion parameters. The proposed model, together with three typical non-square-law *I-V* models, is applied to four different packaging types of GaN HMETs from various manufacturers to verify the broad applicability of the proposed model and its superiority compared to other *I-V* models. The comparison among the models and the measured data are performed on the output characteristics, the transfer characteristics, the output conductance and the transconductance of the four GaN HEMTs. Consistent results have been achieved for all GaN HEMTs regardless the packaging structures, that is, while the traditional non-square-law models show comparable performances without a clear winner, the proposed model is significantly more accurate especially in linear region. The RMS errors of the proposed model is at least 58% lower than that of the second best models, while the over 0.999 $\mathbf{R}^2$ values suggest almost perfect prediction of the actual behaviors of the GaN HEMTs from the proposed model. The proposed model could be a valued addition to the current empirical *I-V* model family and is potentially applied in computer aided circuit simulation of emerging GaN HEMTs.

Acknowledgements

This work is supported in part by the National Natural Science Foundation of China under grants no. 61372015, and the Fundamental Research Funds for the Central Universities under grants no. N150404001.

References

[1] Eastman LF, Mishra UK. The toughest transistor yet [GaN transistors]. Spectrum IEEE 2002;39:28–33.
[2] Curtice WR. A MESFET model for use in the design of GaAs integrated circuits. IEEE Trans Microw Theory Tech 1980;28:448–56.
[3] Shichman H, Hodges DA. Modeling and simulation of insulated-gate field-effect transistor switching circuits. IEEE J Solid-State Circuits 1968;3:285–9.
[4] Rodriguez-Tellez J, England PJ. Five-parameter DC GaAs MESFET model for non-linear circuit design. Circuits Dev Syst IEE Proc G 1992;139:325–32.

[5] Materka A, Kacprzak T. Computer calculation of large-signal GaAs FET amplifier characteristics. IEEE Trans Microwave Theory Tech 1985;33:129–35.
[6] Ahmed MM, Ahmed H, Ladbrooke PH. An improved DC model for circuit analysis programs for submicron GaAs MESFET's. IEEE Trans Electron Dev 1997;44:360–3.
[7] Kacprzak T, Materka A. Compact DC model of GaAs FETs for large-signal computer calculation. IEEE J Solid-State Circuits 1983;18:211–3.
[8] Tellez JR, Al-Daas M, Mezher KA. Comparison of nonlinear MESFET models for wideband circuit design. IEEE Trans Electron Dev 2002;41:288–93.
[9] Islam MS, Islam M, Hasan MR, Islam SMN. An improved nonlinear DC I-V characteristics model for nanometer range GaAs MESFETs. In: TENCON 2009–2009 IEEE Region 10 conference; 2010. p. 1–5.
[10] Ahmed MM. Optimization of active channel thickness of mm-wavelength GaAs MESFETs by using a nonlinear I-V model. IEEE Trans Electron Dev 2000;47:299–303.
[11] Statz H, Newman P, Smith IW, Pucel RA, Haus HA. GaAs FET device and circuit simulation in SPICE. IEEE Trans Electron Dev 1987;34:160–9.
[12] Islam MS, Zaman MM. A seven-parameter nonlinear I-V characteristics model for sub-μm range GaAs MESFETs. Solid State Electron 2004;48:1111–7.
[13] Curtice WR, Ettenberg M. A nonlinear GaAs FET Model for use in the design of output circuits for IEEE transactions on power amplifiers. Microwave Theory Tech 1985;33:1383–94.
[14] Dobes J, Pospisil L. Enhancing the accuracy of microwave element models by artificial neural networks. Radioengineering 2004;13:7–12.
[15] Memon NM, Ahmed MM, Rehman F. A comprehensive four parameters I-V model for GaAs MESFET output characteristics. Solid State Electron 2007;51:511–6.
[16] Mccamant AJ, Mccormack GD, Smith DH. An improved GaAs MESFET model for SPICE. IEEE Trans Microwave Theory Tech 1990;38:822–4.
[17] Angelov I, Zirath H, Rosman N. New empirical nonlinear model for HEMT devices. IEEE Trans Microwave Theory Tech 1992;28:140–2.
[18] Li L, Lin F, Qian W, Khan M, Pei Y. An enhanced AlGaN/GaN HEMTs large-signal model with parameter extraction methodology. In: Asia-Pacific microwave conference; 2015. p. 1–3.
[19] Chen YC, Ingram DL, Yen HC, Lai R, Streit DC. A new empirical I-V model for HEMT devices. IEEE Microwave Guided Wave Lett 1998;8:342–4.
[20] Marcoux NL. Large-signal modeling of GaN HEMT devices for power amplifiers. Dissertations & Theses – Gradworks; 2012. p. 28–33.
[21] Yu ET, Dang XZ, Asbeck PM, Lau SS, Sullivan GJ. Spontaneous and piezoelectric polarization effects in III-V nitride heterostructures. J Vacuum Sci Technol B Microelectron Nanometer Struct 1999;17:1742–9.
[22] Ambacher O, Majewski J, Miskys C, Link A, Hermann M, Eickhoff M, et al. Pyroelectric properties of Al(In)GaN/GaN hetero- and quantum well structures. J Phys: Condens Matter 2002;14:3399.
[23] Baylis CP, Ii. Improved techniques for nonlinear electrothermal FET modeling and measurement validation. Dissertations & Theses - Gradworks. Tampa; 2007. p. 40–8.
[24] Zhao ZQ, Liao DW, Du JF. Effects of surface traps on the breakdown voltage of passivated AlGaN/GaN HEMTs under high-field stress. In: IEEE international conference on solid-state and integrated circuit technology; 2012. p. 1–3.
[25] Jarndal A, Bunz B, Kompa G. Accurate large-signal modeling of AlGaN-GaN HEMT including trapping and self-heating induced dispersion. In: IEEE international symposium on power semiconductor devices and Ic's; 2006. p. 1–4.
[26] Yuk KS, Branner GR, Mcquate DJ. A wideband multiharmonic empirical large-signal model for high-power GaN HEMTs with self-heating and charge-trapping effects. IEEE Trans Microw Theory Tech 2009;57:3322–32.
[27] Lee JW, Webb KJ. A temperature-dependent nonlinear analytic model for AlGaN-GaN HEMTs on SiC. IEEE Trans Microw Theory Tech 2004;52:2–9.
[28] Jarndal A, Aflaki P, Negra R, et al. Large-signal modeling methodology for GaN HEMTs for RF switching-mode power amplifiers design. Int J RF Microwave Comput Aided Eng 2015;21:45–51.
[29] Jarndal A, Aflaki P, Degachi L, et al. Large-signal model for AlGaN/GaN HEMTs suitable for RF switching-mode power amplifiers design. Solid-State Electron 2010;54:696–700.

Jie Yang, received the B.S. degree in Automotive Engineering from Tsinghua University, Beijing, China, the M.S. degree in Mechanical Engineering from North Carolina Agricultural and Technical State University, Greensboro, NC, USA, and the Ph.D. in Electrical Engineering from Syracuse University, Syracuse, NY, USA, in 1998, 2001, and 2007, respectively. He was a senior research engineer with Arkansas Power Electronics International, Inc., and is now a professor with the College of Information Science and Technology, Northeastern University, Shenyang, China. His research interests include wide band-gap semiconductor devices and extreme environment electronics.

Yeting Jia, is currently pursuing her Master's degree in Northeastern University, Shenyang, China, major in Microelectronics and Solid State Electronics. Her current research interests include modeling and applications of GaN HEMT devices.

Ning Ye, received his Ph.D. from Northeastern University, Shenyang, China, in 2010. He is currently a lecturer in Northeastern University, Shenyang, China. His current research interests include GaN and SiC power devices.

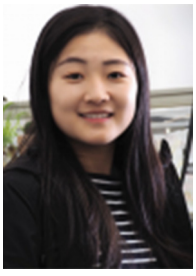

Shuo Gao, is currently pursuing her Master's degree in Electric Circuits and Systems in Northeastern University, Shenyang, China. Her current research interests include high temperature circuit simulation and design based on wide bandgap devices.